ICARUS **129,** 421–439 (1997)
ARTICLE NO. IS975796

Prediction of Water in Asteroids from Spectral Data Shortward of 3 μm

Erzsébet Merényi[1]

Lunar and Planetary Laboratory, University of Arizona, Tucson, Arizona 85721
E-mail: erzsebet@lpl.arizona.edu

Ellen S. Howell

Department of Geology, University of Puerto Rico, Managüez, Puerto Rico 00681-5000

and

Andrew S. Rivkin and Larry A. Lebofsky

Lunar and Planetary Laboratory, University of Arizona, Tucson, Arizona 85721

Received May 22, 1996; revised May 12, 1997

Spectra of many asteroids display a 3 μm absorption feature that has been associated with the presence of water of hydration in clays or hydrated salts. Detection of this feature, however, is difficult through the Earth's atmosphere for various reasons. Correlations were sought and detected between the 3 μm absorption band and features shortward of 3 μm, which enabled us to construct a tool for the prediction of water in asteroids from the shorter wavelength part of the spectrum. Such a prediction tool can help concentrate observing resources to those objects most likely to have water. Artificial neural network techniques were used for the investigation of the above correlations and for the prediction of the hydration state of objects. We can predict the presence of water from the <3 μm spectral window with a high, approximately 90% success rate for spectra for which prediction is possible. However, for about half the spectra in this study, no decision could be made, for lack of sufficient training information. We expect this situation to improve steadily as new data become available.

1. WATER DETECTION ON ASTEROIDS

An absorption feature at 3 μm is present in spectra of objects that contain OH and/or H_2O. On asteroids, this feature has been attributed to water of hydration in clays or hydrated salts like those present in carbonaceous meteorites. We are looking for correlations that may exist between the 3 μm water band and other, much more subtle, spectral features shortward of 3 μm. If such associated features are detected, then it may be possible to construct a tool with which the presence of a 3 μm water band could be predicted from shorter wavelength observations, with high probability. Due to low flux levels and terrestrial absorption it is often difficult to detect the presence of the 3 μm water band. Prediction capability using shorter-wavelength data would allow us to more easily obtain observations and enable the economization of the 3 μm band observations by focusing on those objects which are most likely to have such a band. The correlations that we investigate are also relevant for taxonomy development by incorporating water as a significant compositional feature in the asteroid classifications.

Vilas (1994) presented a discussion of possible relationships between the 3 μm feature and shorter wavelength features, though little formal identification has been made so far. Vilas found an 80% correlation between a feature at roughly 0.7 μm, due to an Fe^{2+}–Fe^{3+} charge transfer absorption, and 3 μm features. However, this is not a perfect correlation as the 0.7 μm feature occurs in the absence of the 3 μm absorption and it is absent when the 3 μm band is present, in some cases. It does not work at all for the enigmatic hydrated E- and M-class asteroids (called W-class asteroids by Rivkin *et al.* (1995)), which have no 0.7 μm feature.

Taxonomies have not yet begun to include data taken at 3 μm. Besides the tentative formation of the W class to split the hydrated M asteroids from the anhydrous ones, and the suggestion that asteroids with known hydration state have an ''h'' or ''n'' appended to their spectral class

[1] Also at Central Research Institute for Physics, Hungarian Acad. Sci., Budapest, Hungary.

0019-1035/97 $25.00

by Burbine and Bell (i.e., 4 Vesta becomes a Vn, 1 Ceres becomes a Gh) (Burbine and Bell 1993), no spectral classifications have included these data either. As we have 3 μm data on nearly 100 asteroids, the time to start including these data in taxonomic work seems at hand.

Vilas (1994) has shown that any correlating features are likely to be very subtle. We are employing an advanced computational method, an Artificial Neural Network (ANN), in an attempt to detect any correlations. This technique has helped in an earlier taxonomy development to separate olivine rich and pyroxene rich spectral subclasses within the S class (Howell *et al.* 1994). The existence of such compositionally meaningful taxonomic subclasses had been suspected by many workers (e.g., Chapman 1987, Barucci *et al.* 1987, Burbine 1991, Gaffey *et al.* 1993) yet clear formal detection eluded the conventional methods.

In this study we search for the above correlations by classification of 14-color data, mostly C, G, E, M, P, D, and T classes, in the 0.33–3.35 μm range. The basic approach is to train a neural network classifier to recognize "wet" (that is, with a 3 μm feature) objects, first based on spectra that contain the 3 μm band. If this is successful then we truncate the spectra by removing the 3 μm band, i.e., cut off the last few spectral points, and repeat the training from scratch. This means erasing the memory of the network, but using the same spectra for training samples as before except now in their truncated form. The idea is that if the classifier can learn to identify the wet objects from the shortened data and based on that training it can make reasonable predictions for unseen spectra, then a feature or features in the visible or near-infrared (VIS–NIR) exist(s) which co-exist(s) with the 3 μm water band and thus can be used as indicator(s) for the presence of a 3 μm feature. The data are described in Section 2. Details of this analysis are given in Section 3. We discuss results in Sections 4 and 5, and further investigate correlating features in Section 6.

2. OBSERVATIONS IN THE 0.3–3.5 μm RANGE

The data used here are combined from different observations as illustrated in Fig. 1. Searches for water of hydration were conducted at the IRTF by Jones, Lebofsky, Feierberg, Howell, Britt, and Rivkin (Lebofsky 1980, Feierberg *et al.* 1981, 1985, Jones *et al.* 1990, Lebofsky *et al.* 1990, Howell *et al.* 1992, Britt *et al.* 1992, 1994, Howell 1995, Rivkin *et al.* 1995). Broadband J, H, and K photometry was obtained along with the narrowband 2.95, 3.12, and 3.25 μm filters. Higher resolution data taken by Jones were transformed to these filters using the transmission curves measured in the laboratory. The visible data were taken from the 8-color survey (Zellner *et al.* 1985, Tholen 1984) or, when necessary, UBV photometry (Tedesco 1989).

These spectral data are all expressed as relative reflectance, normalized to 1.0 at 0.55 μm. For those objects

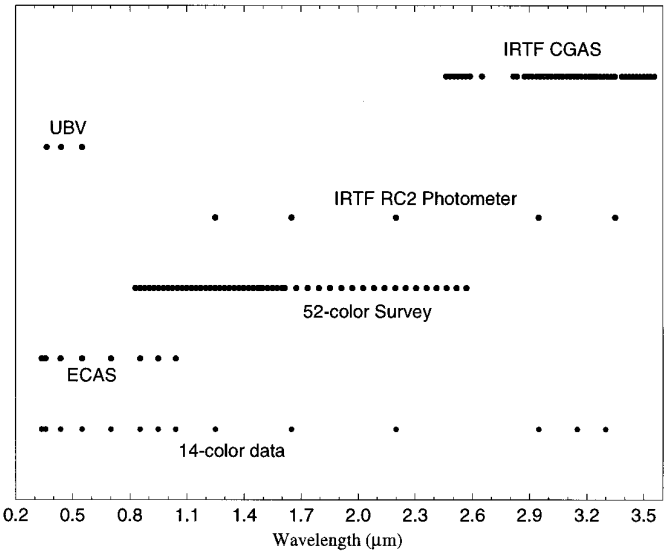

FIG. 1. The wavelength positions for the 14-color data and the data sets that went into their construction are shown here. Problems with the 3.12 μm filter led to the dropping of this point to form 13-color data.

observed during the 52-color survey, the spectral overlap allowed scaling of the J, H, and K points relative to V (0.55 μm). Small errors may exist due to different rotational phases observed in different parts of the spectrum. Several objects were observed at V, J, H, and K sequentially, providing a consistent normalization. However, in some cases, scaling the near-infrared data was done empirically by extrapolating the 8-color data and JHK data and obtaining the best spectral slope match. The 80 different objects for which 126 such combined spectra are presently available are listed in Table I. To take into account the observational uncertainties and thus the effect of the noise on the classification, 10 more spectra were generated for each original by adding random Gaussian noise, based on the uncertainties. A large part of the analysis was done on the resulting 1386 spectra. Figure 2 illustrates the variety of spectral shapes that are equally probable on the basis of the errors. The well behaved case (Fig. 2a) and the moderate case (Fig. 2b) are examples of the typical situation. Case 2b is apparently noisy but the 3 μm water band is consistently there in every possible variant of the spectrum. Figure 2c shows a case when the error bars are large enough to make the 3 μm band uncertain. Fortunately there are only a few such observations.

One particular problem, unfortunately, arose with these data. It has been discovered that the 3.12 μm point within the 3 μm water band shows measurement inconsistencies over a large period of time. This filter apparently degraded with time and became unusable in later data sets. We have been unable to reconstruct the data, therefore we had to

TABLE I
Asteroids for which 3-μm Data Has Been Obtained

	Asteroid	Taxonomic Class	Date Observed	Band Depth (%)			Water?	Reference
1	Ceres	G	2 Nov 1984	23.53	±	1.59	Wet	2
1	Ceres	G	mean[a] 1987	22.82	±	2.00	Wet	3
1	Ceres	G	24 Apr 1987	23.50	±	3.14	Wet	3
1	Ceres	G	24 Apr 1987	41.59	±	0.61	Wet	3
1	Ceres	G	24 Apr 1987	24.71	±	3.84	Wet	3
1	Ceres	G	25 Apr 1987	20.39	±	3.50	Wet	3
1	Ceres	G	22 Aug 1988	16.58	±	1.72	Wet	2
2	Pallas	B	mean 1977-1978	13.91	±	4.06	Wet	5
2	Pallas	B	mean 1987	16.54	±	0.52	Wet	3
2	Pallas	B	21 Apr 1987	19.31	±	2.93	Wet	3
2	Pallas	B	21 Apr 1987	16.74	±	1.57	Wet	3
2	Pallas	B	24 Apr 1987	16.03	±	5.28	Wet	3
2	Pallas	B	25 Apr 1987	16.42	±	1.27	Wet	3
2	Pallas	B	25 Apr 1987	15.70	±	1.28	Wet	3
2	Pallas	B	25 Apr 1987	17.29	±	1.26	Wet	3
2	Pallas	B	25 Apr 1987	16.98	±	1.26	Wet	3
2	Pallas	B	25 Apr 1987	16.66	±	1.27	Wet	3
4	Vesta	V	24 Dec 1983	0.00	±	1.05	Dry	1
5	Astraea	Sp	24 Apr 1987	5.52	±	3.57	Dry	3
5	Astraea	Sp	24 Apr 1987	7.85	±	3.39	Dry	3
10	Hygiea	C	20,21 Mar 1983	13.10	±	0.98	Wet	1
10	Hygiea	C	8 Dec 1986	1.61	±	2.01	Dry	3
10	Hygiea	C	1 Feb 1988	11.05	±	4.15	Wet	3
13	Egeria	G	23 Dec 1983	22.54	±	1.96	Wet	1
13	Egeria	G	3 Oct 1987	36.81	±	5.53	Wet	3
16	Psyche	M	25 Apr 1987	0.02	±	1.75	Dry	3
16	Psyche	M	30 Dec 1991	0.01	±	12.34	Dry	4
18	Melpomene	SoT,S	24 Apr 1987	4.53	±	2.24	Dry	3
19	Fortuna	G	8,15,29 Oct 1978	20.18	±	3.10	Wet	5
24	Themis	C	2 Nov 1984	9.61	±	2.34	Wet	2
31	Euphrosyne	C	24 Dec 1983	3.55	±	0.96	Dry?	1
36	Atalante	C	23,24 Dec 1983	14.39	±	6.59	Wet	1
44	Nysa	E	30 Dec 1991	16.66	±	9.08	Wet	4
44	Nysa	E	15,18 Aug 1993	12.83	±	6.17	Wet	4
50	Virginia	P	30 Dec 1991	22.39	±	9.29	Wet	4
51	Nemausa	CU	21 Feb 1978	13.51[b]	±	4.63	Wet	5
51	Nemausa	CU	2 Nov 1984	46.71	±	6.11	Wet	2
51	Nemausa	CU	3 Oct 1987	44.64	±	5.31	Wet	3
52	Europa	CF	20-22 Mar 1983	2.74	±	2.18	Dry	1
52	Europa	CF	3 Oct 1987	5.61	±	6.43	Dry	3
55	Pandora	M	3 Feb 1988	17.30	±	8.99	Wet	3
55	Pandora	M	29 Dec 1991	4.44	±	4.76	Dry?	4
64	Angelina	E	29 Dec 1991	5.33	±	10.80	Wet?	4
65	Cybele	P	2,3 Nov 1984	0.00	±	3.31	Dry	1,2

TABLE I—*Continued*

	Asteroid	Taxonomic Class	Date Observed	Band Depth (%)			Water?	Reference
70	Panopaea	C	12 Mar 1979	35.41	±	12.93	Wet	5
70	Panopaea	C	15,18 Aug 1993	10.08	±	4.51	Wet	8
72	Feronia	TDG	8,29 Oct 1978	8.07	±	5.81	Wet?	5
72	Feronia	TDG	22,23 Oct 1985	5.91	±	2.42	Wet?	2
74	Galatea	C	23,24 Dec 1983	3.45	±	1.88	Dry?	1
75	Eurydike	M	15 Aug 1993	0.00	±	5.75	Dry	4
77	Frigga	MU	15 Aug 1993	10.70	±	3.31	Wet	8
87	Sylvia	P	22,23 Oct 1985	8.11	±	1.72	Dry?	2
88	Thisbe	C	mean 1978,1979	0.00	±	17.91	Dry[c]	5
92	Undina	M	1 Oct 1988	46.03	±	8.52	Wet	3
92	Undina	M	15,18 Aug 1993	9.99	±	2.78	Wet	4
114	Kassandra	T	22,23 Oct 1985	4.51	±	9.65	Wet?	3
114	Kassandra	T	9 Dec 1986	0.00	±	0.83	Dry	2
114	Kassandra	T	9 Dec 1986	0.98	±	0.82	Dry?	2
114	Kassandra	T	30 Dec 1991	0.00	±	13.08	Dry	9
130	Elektra	G	2 Feb 1988	25.32	±	6.33	Wet	3
139	Juewa	CP	20-22 Mar 1983	2.02	±	4.79	Dry?	1
139	Juewa	CP	29 Dec 1991	0.57	±	5.70	Dry	9
148	Gallia	GU	1 Feb 1988	4.19	±	7.89	Dry	3
148	Gallia	GU	30 Dec 1991	0.00	±	12.88	Dry	9
163	Erigone	C	11 Feb 1992	16.90	±	6.11	Wet	7
185	Eunike	C	15,18 Aug 1993	4.91	±	5.04	Dry?	8
190	Ismene	P	10 Feb 1991	0.00	±	8.71	Dry	9
201	Penelope	M	15,18 Aug 1993	5.24	±	2.31	Wet	4
216	Kleopatra	M	18 Aug 1993	3.42	±	4.71	Dry	4
233	Asterope	T	2,3 Nov 1984	6.85	±	2.50	Dry	2
233	Asterope	T	22,23 Aug 1988	4.96	±	1.63	Dry	2
240	Vanadis	C	15,18 Aug 1993	14.27	±	8.82	Wet	8
243	Ida	S	28-30 Dec 1991	11.76	±	12.63	Dry	9
247	Eukrate	CP	24 Dec 1983	2.07	±	2.61	Dry	1
304	Olga	C	11 Feb 1992	9.45	±	39.33	Dry[c]	7
308	Polyxo	T	2 Nov 1984	20.93	±	2.37	Wet	2
313	Chaldea	C	2 Feb 1988	28.38	±	7.58	Wet	3
324	Bamberga	CP	23,24 Dec 1983	9.08	±	0.97	Wet	1
324	Bamberga	CP	2 Oct 1987	29.69	±	6.78	Dry	3
324	Bamberga	CP	4 Feb 1988	6.53	±	7.67	Dry	3
335	Roberta	FP	11 Feb 1992	0.00	±	10.36	Dry	7
336	Lacadiera	D	11 Feb 1992	7.39	±	7.85	Wet?	6,7
336	Lacadiera	D	29,30 Dec 1991	34.06	±	8.39	Wet	6
344	Desiderata	C	22 Mar 1983	19.18	±	4.12	Wet	1
349	Dembowska	R	22 Nov 1977	2.93	±	3.65	Dry	5
375	Ursula	C	3 Oct 1987	0.00	±	13.71	Wet?	3
386	Siegena	C	20-22 Mar 1983	24.95	±	2.19	Wet	1
409	Aspasia	CX	3 Feb 1988	10.10	±	6.55	Wet?	3

eliminate that point (the last but one point in Fig. 1) from the analysis. Thus the spectra are reduced to 13 points.

By convention, in this paper we will call the set of spectra over the full 0.33–3.35 μm range "13-color" data, and the spectra truncated to contain only the spectral range shortward of 3 μm "11-color" data. These channel selections are illustrated in Fig. 3, along with three others that were used in addition to the 13- and 11-color data sets, to

TABLE I—*Continued*

	Asteroid	Taxonomic Class	Date Observed	Band Depth (%)			Water?	Reference
409	Aspasia	CX	11 Feb 1992	7.34	±	6.61	Dry?	7
409	Aspasia	CX	15,18 Aug 1993	6.52	±	3.46	Dry?	8
410	Chloris	C	29,30 Apr 1983	25.27	±	3.12	Wet	1
429	Lotis	C	15,18 Aug 1993	0.00	±	24.93	Dry	8
444	Gyptis	C	15,18 Aug 1993	0.00	±	7.12	Dry	8
449	Hamburga	C	10 Feb 1991	0.00	±	24.91	Dry	9
497	Iva	M	18 Aug 1993	0.40	±	5.78	Dry	4
505	Cava	FC	2 Feb 1988	18.93	±	6.97	Dry	3
505	Cava	FC	30 Dec 1991	7.20	±	11.17	Dry	9
511	Davida	C	30 Apr 1983	16.03	±	1.89	Wet	1
511	Davida	C	21 Apr 1987	15.17	±	3.02	Wet	3
511	Davida	C	24 Apr 1987	22.20	±	4.91	Wet	3
511	Davida	C	25 Apr 1987	11.81	±	4.46	Wet	3
511	Davida	C	25 Apr 1987	7.77	±	5.36	Wet	3
532	Herculina	S	21 Apr 1987	3.78	±	1.01	Dry	3
554	Peraga	FC	16,17 Nov,13 Dec 1977	0.00	±	5.78	Dry	5
566	Stereoskopia	C	10 Feb 1991	0.67	±	12.99	Dry	9
570	Kythera	T	23 Aug 1988	14.30	±	1.72	Wet	2
572	Rebekka	M	29,31 Dec 1991	0.00	±	28.30	Dry	4
596	Scheila	PCD	10 Feb 1991	0.00	±	7.40	Dry	9
620	Drakonia	E	18 Aug 1993	2.60	±	12.77	Dry	4
623	Chimaera	XC	2 Oct 1990	2.48	±	21.70	Dry	9
654	Zelinda	C	15,18 Aug 1993	8.45	±	7.44	Wet?	8
704	Interamnia	F	22 Oct 1984	15.59	±	2.04	Wet?	2
704	Interamnia	F	25 Apr 1987	12.35	±	8.41	Dry?	3
704	Interamnia	F	30 Dec 1991	5.72	±	12.60	Dry?	9
721	Tabora	D	22-23 Oct 1985	0.93	±	7.12	Dry	2
748	Simeisa	P	24 Aug 1988	0.00	±	8.35	Dry	2
773	Irmintraud	D	2 Oct 1990	4.75	±	15.03	Wet?	6,7
773	Irmintraud	D	23 Oct 1985	2.28	±	5.44	Dry	2
776	Berbericia	C	23,24 Dec 1983	25.28	±	2.18	Wet	1
785	Zwetana	M	30 Dec 1991	0.00	±	12.25	Dry	4
796	Sarita	M	29 Dec 1991	0.00	±	7.46	Dry	4
849	Ara	M	18 Aug 1993	2.19	±	6.79	Dry	4
944	Hidalgo	D	2 Oct 1990	0.00	±	17.71	Dry	6,7
1172	Aneas	D	22 Aug 1988	0.00	±	4.46	Dry	2
1467	Mashona	GC	10 Feb 1991	88.06	±	6.54	Wet	9
1867	Deiphobus	D	22-24 Aug 1988	0.75	±	4.81	Dry	2

Note. Band depth is measured at 2.95 μm. Asteroids with no feature have been shown with a band depth of zero and no errors. Asteroids with insufficient signal-to-noise to determine a definite hydration state are shown with a question mark. Keys to references: (1) Feierberg *et al.* 1985, (2) Lebofsky *et al.* 1990, (3) Jones *et al.* 1990, (4) Rivkin *et al.* 1993, (5) Lebofsky 1980, (6) Howell 1995, (7) Observations by D. T. Britt, (8) Observations by D. T. Britt and A. S. Rivkin, previously unpublished, (9) Observations by E. S. Howell previously unpublished.

[a] Mean does not include the observation on 24 Apr 1987 with band depth of 41.59%.

[b] Band measured at 3.25 μm, spectrum is consistent with other observations.

[c] Large uncertainties, designation uncertain.

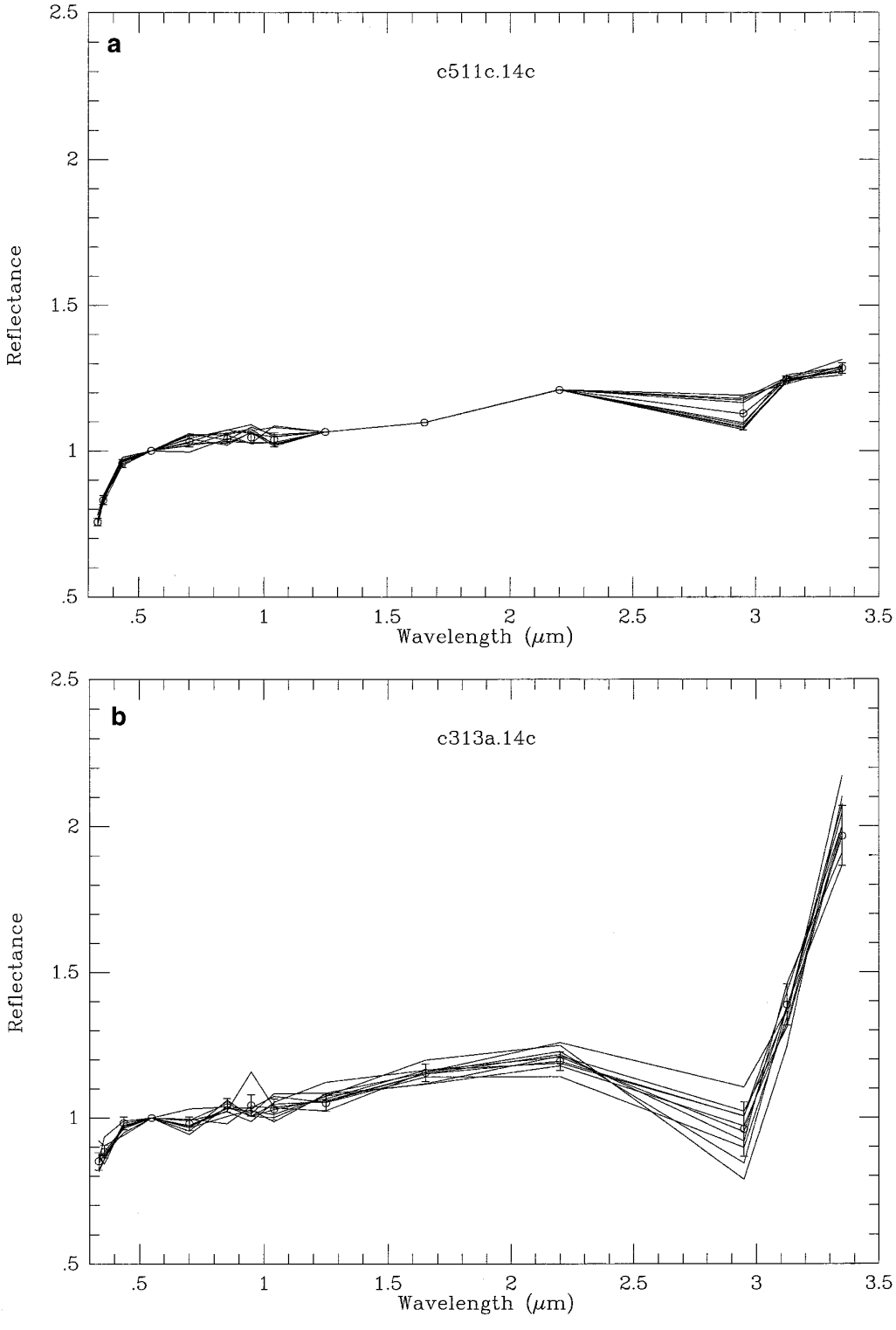

FIG. 2. Possible spectral variation within observational error. These spectra were generated by adding random Gaussian noise to the observed values based on the error bars. All spectral shapes are equally probable. The spectra are normalized to 1.0 at 0.55 μm, so the error for that point is zero. (a) Well behaved case, with small errors, 511 Davida. (b) A moderate case, 313 Chaldea. (c) An extreme case, 623 Chimaera.

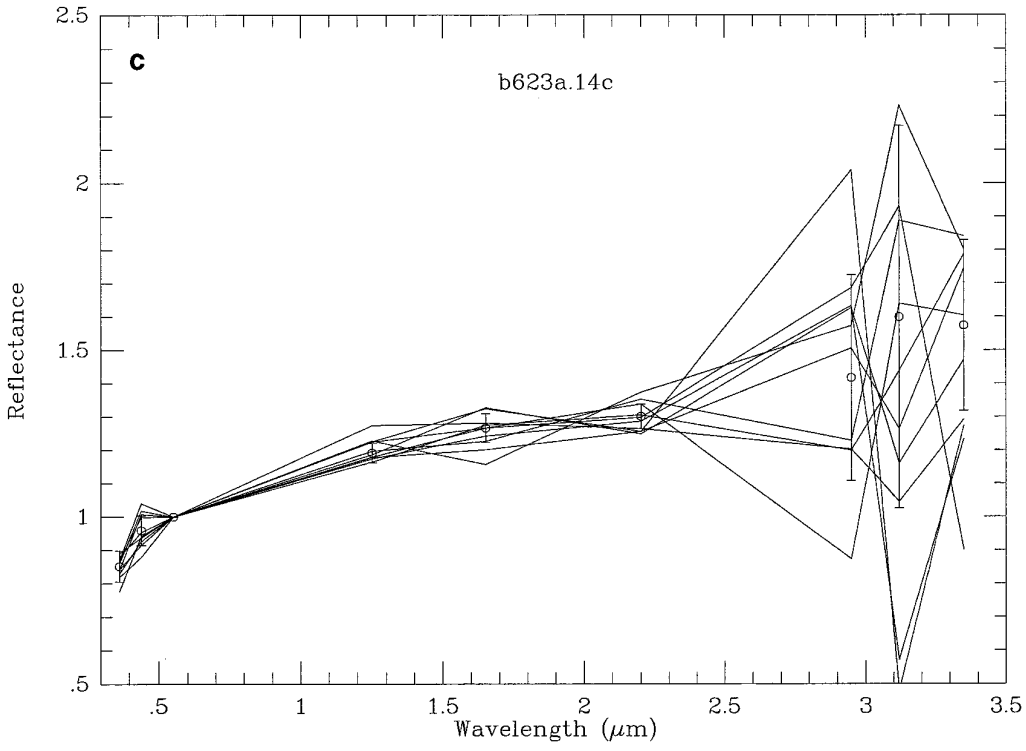

FIG. 2—*Continued*

investigate what features make water prediction possible from the shorter wavelengths.

3. METHODOLOGY AND ANALYSIS TECHNIQUES

To systematically investigate whether a consistent relationship exists between the 3 μm water band and any other features shortward of 3 μm we took the following steps. First we wanted to see if these spectra showed a grouping by water, using all 13 points, and if so, whether the data showed the same or similar grouping without the 3 μm band. Next we trained an ANN classifier to learn the water designation of some of the objects for which we had firm knowledge and performed a supervised classification on the 13-color data. We repeated this for the 11-color data, using the truncated spectra of the same objects for training. The key idea is that if we get a reliable prediction rate for the 13-color data then we know that the ANN was capable of generalizing from the training spectra and was able to identify the wet objects that were not part of the training set. We then truncate the spectra and train the ANN to recognize the same known wet and dry objects as before. Now, if this training provides a good prediction rate for unseen spectra from their truncated, 11-color, spectra then there must be some feature that is characteristic and co-occurring with the 3 μm water band. The term unseen spectra means spectra that were not included in the training set.

We describe the details of these steps below after a short summary on ANNs in general and a somewhat more detailed explanation of the Self-Organizing Neural Network paradigm.

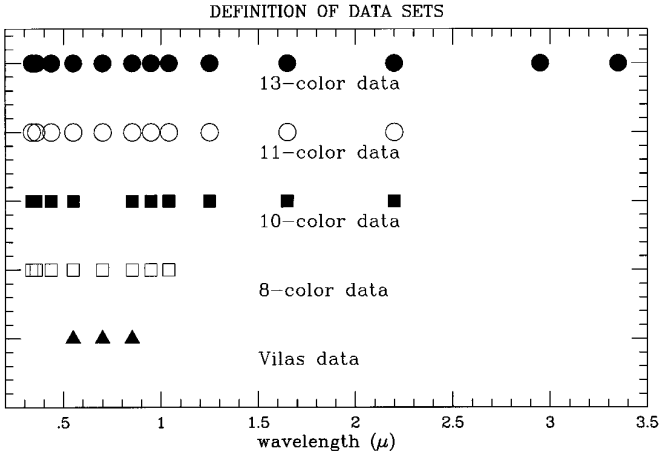

FIG. 3. The spectral channel selections used in this study. The 13-color and the 11-color data sets were used to create a tool for the prediction of the hydration state from the wavelength range shortward of 3 μm. The other three data sets helped assess the relative contributions of various parts of the spectrum to the identification of the hydration state.

3.1. Artificial Neural Networks

An ANN is an architecture which is intended to simulate the structure and functions of the biological nervous sys-

tem. Neurobiologists use ANNs to model cognitive processes; data analysts look to them as a next generation computing device and mathematical tool for data exploitation. Such a system, similar to our brain, learns to solve problems from examples. These systems can be described as massively parallel, finely distributed, and learning machines. Massively parallel, because a large number of identical and densely interconnected processors—the equivalents of the nerve cells—work simultaneously, creating an impressive communication bandwidth. These processors, called the Processing Elements (PEs), are uniform and all perform the same very simple function. Tasks are broken down to elementary subtasks on this primitive level, for ultimately fine distribution among the PEs. Figure 4 illustrates the most important details of an ANN. The distribution of a task among the PEs is no longer done by scheduling as in a regular distributed computer network where the individual processors are non-uniform, very complex functional units (different computer CPUs). In an ANN, distribution of a task to the level of individual PEs happens by learning, in a similar way as in our brain.

The learning takes place in the connection weights, which are the analogs of the synaptic strengths between nerve cells. For example, if our task is to classify spectral patterns, the values from the spectral channels are introduced at the input layer, one spectrum at a time, each channel assigned to one input PE. Each PE in the subsequent layer receives a weighted sum of the inputs and performs on it a given simple function, as described in Fig. 4. The resulting output value is passed onto the PEs in the next layer, which will in turn process them as their input. Finally, after as many time steps as there are layers, the output layer has a response to our spectral pattern. This we can interpret as a class prediction in an encoded form. For example, if we want to train the ANN to recognize five classes of spectra, then the output layer will have five PEs and class A can be represented by a five-dimensional vector (1, 0, 0, 0, 0), class B by (0, 1, 0, 0, 0), ..., etc., at the output. Naturally, at the beginning the ANN will not yet have learned any class designations and the output will be quite random. At this point, the teacher gives feedback to the network, by presenting the correct class label. Based on the difference between the correct label and the actual prediction, the connection weights throughout the entire ANN are then modified in such a way that next time when this pattern is shown, a more accurate prediction occurs. The modification of the weights is governed by a learning rule, which is one of the defining components of an ANN. The training patterns are shown this way, along with their correct class labels, many times to the ANN, until correct designations result for all training patterns. Then the network is trained and its knowledge is stored in the weights. A well-trained ANN can generalize from this knowledge and make reasonable predictions for patterns that were not part of the training set. The quality of the prediction for unseen patterns depends on the quality of the training including the number of training patterns and how well the training set represents the range and details of the population in the analysis.

ANNs are well suited for problems that are easily described by examples and which would be extremely difficult to define analytically. For example, it would be rather challenging to define rules for the characteristics of a given spectral class, say A-type asteroids, whereas selecting a set of representative A-type asteroid spectra is not very difficult. Typically, ANNs excel in solving problems in which humans are superior to computers, such as pattern recognition. ANNs have been gaining popularity in recent years not only because of the high speed that the parallel architecture offers but just as importantly because their capabilities are superior to classical methods in classifying noisy and complex data such as observed reflectance spectra of geological surfaces. Excellent textbooks on the details of many ANN paradigms are, e.g., Pao (1989) and Hayken (1995). Some applications of ANNs in the area of spectral analysis problems are, e.g., Benediktsson *et al.* (1990, 1994), Hepner *et al.* (1990), Merényi *et al.* (1993, 1996), Ninomiya and Sato (1990), Paola and Schowengerdt (1994), and Wang and Civco (1995).

3.1.1. The self-organizing map, for clustering. The internal structure of a data set is often investigated by clustering. As the dimensionality of the data (such as the number of spectral bands) increases the difficulty in obtaining a good, reliable cluster map increases, too. In addition, visualization of the higher-dimensionality clusters and their interrelationships becomes a great challenge. The frequently used scattergrams or pairwise Principal Component planes are only partial and unsatisfactory solutions beyond four–five dimensions.

The Self-Organizing Map (SOM) is an ANN paradigm that offers an elegant solution (Kohonen 1988). It maps, in an unsupervised learning procedure, the n-dimensional input patterns onto a two-dimensional lattice of PEs in such a way that similar patterns land closer to one another in all directions than dissimilar ones. More details will follow in Section 4, through our concrete examples. This mapping occurs via competitive learning among the PEs in the lattice: each PE tries to adjust its weights such that those become similar to the incoming pattern. The PE with the most similar set of weights wins, and the input pattern will be mapped to that PE. Any adjustment of weights in one PE affects its neighborhood, which comprises the adjacent PEs in the lattice. The neighbor cells will also undergo weight changes according to the learning rule of the SOM and to those changes in the center PE, which results in a neighborhood of similar but somewhat different ordered patterns. This neighborhood then attracts the pat-

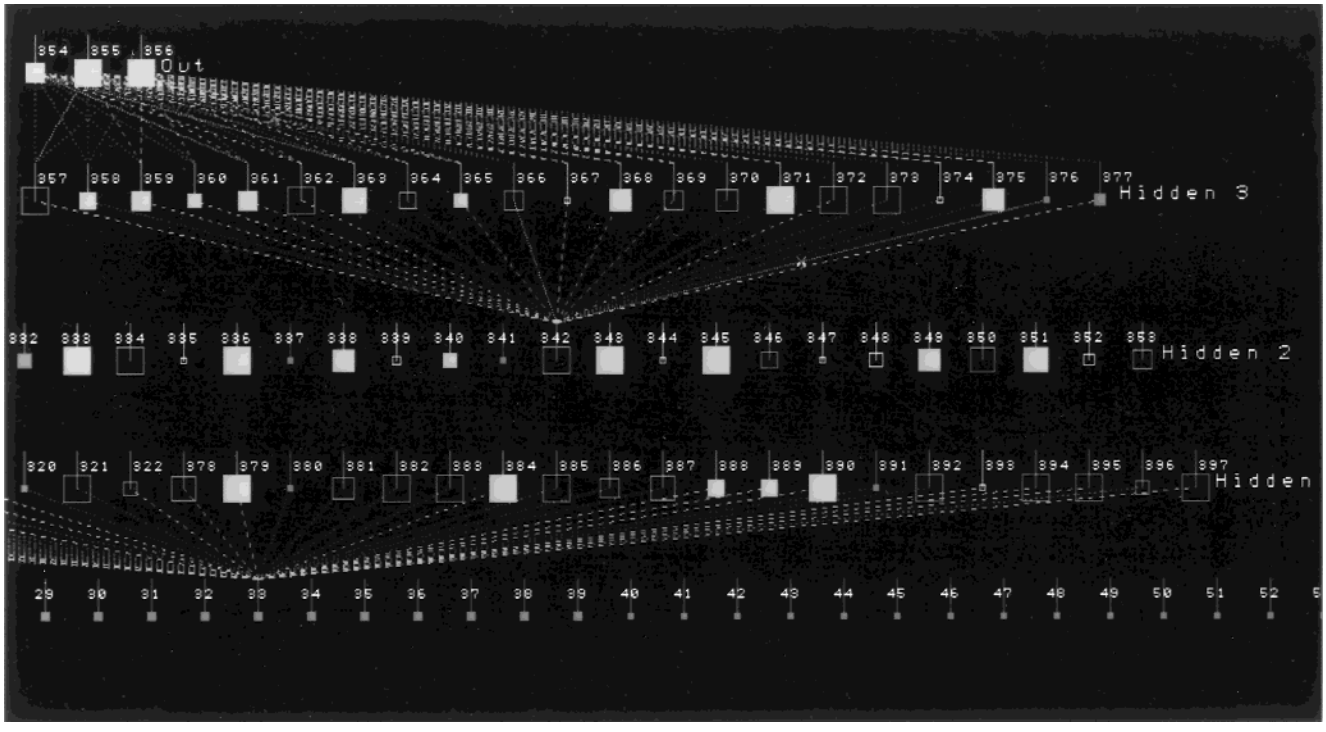

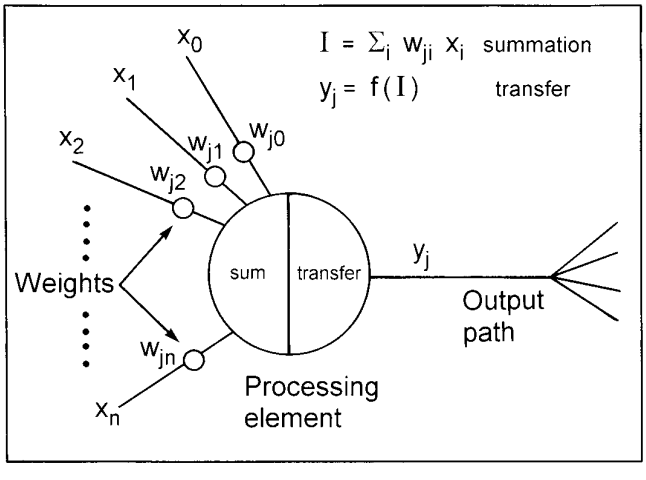

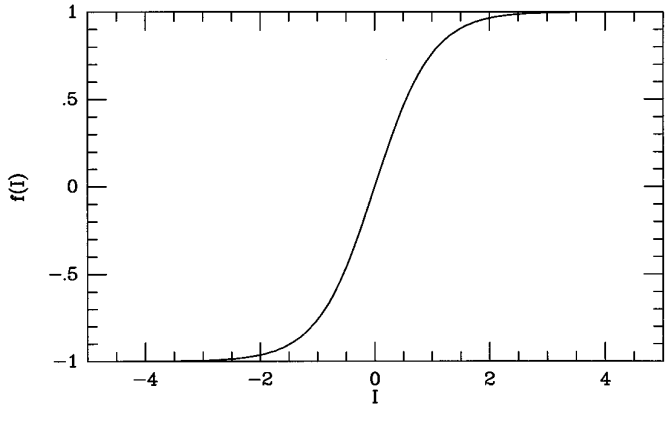

FIG. 4. (Top) An example of the most common feed-forward ANN paradigm, the Back Propagation network. This network consists of 5 layers of Processing Elements (PEs), one input (bottom), three hidden (next three), and one output layer (top). The PEs are represented by the square boxes, the size and color of which is related to the internal state of the PE. All PEs in any layer are connected to all PEs in the next layer. PEs within a layer are not connected. Only several of the connections are illustrated here by the dashed lines. The connection strengths (weights) can change when the ANN is learning, according to a learning rule. Data are introduced at the input layer and processed by the subsequent layers in subsequent time steps. The output from the PEs in one layer forms the input to the PEs in the next layer. Information flow in this ANN is one-directional, from bottom to top, hence the name feed-forward. The PEs all have the structure that is shown on bottom left and perform the same simple function. Training of an ANN is the adjustment of the connection weights based on the difference between the ANNs answer at its output layer and the correct answer, during repetitious presentation of sample data along with the correct answers to them. Many different paradigms have been invented, for various types of problems. The connection pattern, the transfer function and the learning rule are the defining components of an ANN paradigm. Image taken with permission from the user interface screen of NeuralWorks Professional II software package, NeuralWare, Inc. (Bottom left) The structure of a single Processing Element, the analog of the biological nerve cell. The input connections from other PEs and the weights associated with them are the analogs of the dendrites and the synaptic strengths of the nerve cell, respectively. The nucleus of the PE applies a function to the sum of the weighted inputs according to the formula. The function *f* is generally non-linear, and is usually of a sigmoid shape (bottom right). The output, similar to the inputs, is a continuous value not just a 1/0 binary signal. Figure copied with permission from NeuralWare, Inc. (1991).

terns that are most similar to the one that was mapped to the center PE. The learning formulas for the SOM are described in NeuralWare, Inc. (1991). During learning, as patterns are shown many times, the winning PE for a particular pattern may change until no other PE can produce a better approximation of that pattern. This happens simultaneously for all input patterns until the process stabilizes and ''migration'' of the mapped patterns no longer takes place.

This is a topological mapping: the similarity relationships (the relative spatial ordering of the patterns in n-dimensional space) are preserved and reflected in this two-dimensional lattice but the Euclidean distances are not proportional to the measure of similarities between patterns. The degree of similarity between groups of patterns is encoded in the connection weights at the end of the unsupervised training. This information can be visualized as walls of certain heights between groups of patterns. The walls delineate cluster boundaries. The higher the wall, the larger the dissimilarity between the separated groups. Howell *et al.* (1994) showed such similarity maps for 8-color asteroid spectra and for 60-color spectra combined from the ECAS and the 52-color survey. This clustering technique reproduced the Tholen taxonomy for the 8-color survey and detected and visualized additional structure in the 60-color data compared to previous analyses of the same data.

3.1.2. A hybrid ANN for supervised classification. Establishing a cluster structure of the data is helpful in comparisons with previous knowledge about the same data and in setting up classes that are meaningful for the particular problem under research. It can also be very useful in influencing—constraining—a subsequent supervised training. With growing spectral dimensionality and larger numbers of classes, the possibility of inconsistent class labeling at the time of setting up the training classes increases because of the increasingly complex interrelationships of the patterns. When a system has its own internal ''view'' of the similarities among patterns (such as that encoded in the SOM) it can refuse to learn associations that are inconsistent with that view. For example, take two spectra that are mapped very close to one another in the SOM and are both part of a group that is separated from another group of spectra. Training a system that has access to this knowledge, to label the spectra in the first group as type A and all spectra in the second group as type B except one for which we want to impose the label A, is likely to refuse to associate type A with that sepctrum closely clustered with the B types. Without the knowledge of the cluster structure, some systems (e.g., the powerful and popular Back Propagation ANN paradigm) may simply ''memorize'' the inconsistent pieces of information, which would lead to poor inferences about the general properties of spectral classes. In addition, the predetermined clusters also help derive class properties more effectively from a smaller amount of training samples than other systems would without this knowledge.

Instead of using an entirely separate ANN for supervised training (such as Back Propagation, which is frequently the choice), we utilize the knowledge in the SOM by coupling it with another ANN. The second ANN has the SOM output as its input and one additional layer for output. Each PE in that output layer is connected to all PEs in the SOM (see Fig. 5 in Howell *et al.* 1994). The learning rule of the second ANN is called the Widrow–Hoff rule and the specific implementation is found in NeuralWare (1991).

4. THE INTERNAL RELATIONS IN THE DATA AS SEEN FROM UNSUPERVISED CLASSIFICATION

Our diverse collection of 1386 spectral shapes were fed into a self-organizing ANN, which has unique capabilities for organizing the incoming data according to similarities among them, in an unsupervised learning process as described in Section 3.1.1. The data points (spectra) are mapped onto a two-dimensional grid such that less similar ones will be farther apart in both directions. We remind the reader of the topological nature of this map, i.e. that the closeness in similarity of spectral groups is not linearly proportional to their Euclidean distance. To illustrate what happens as a result of this self-organization, Fig. 5a shows about 400 randomly selected spectra from our data set which were entered to the SOM along with the remaining 1000 or so spectra, and Fig. 5b shows the output, which is the same 1386 spectra neatly organized into groups of similar shapes. The two-dimensional SOM in this case consisted of 20×20 PEs, with an input layer of 13 and 11 PEs for the 13- and the 11-color data, respectively. Since very similar spectra can be mapped onto the same PE in the SOM, several spectra may be plotted on top of one another in Fig. 5b.

Figure 6 is essentially the same map viewed in a more complex way. We compare here the SOM of the 13-color data with the SOM of the 11-color data. On these maps a small square is plotted in the PE grid location where the corresponding spectrum was mapped by the ANN. Each grid point is represented in these figures by a 4×4 patch of small squares so that each spectrum that is mapped on the same PE can appear as a separate square as long as there are not more than 16 spectra to one PE. We have chosen the 4×4 squares per grid cell resolution because all PEs had less than 16 spectra mapped to them. The cluster boundaries are marked by the white fences, which were computed from the SOM weights as described in 3.1.1. The thickness of the lines indicates the degree of dissimilarity between the groups of spectra. The wider the line, the less similar the separated groups are.

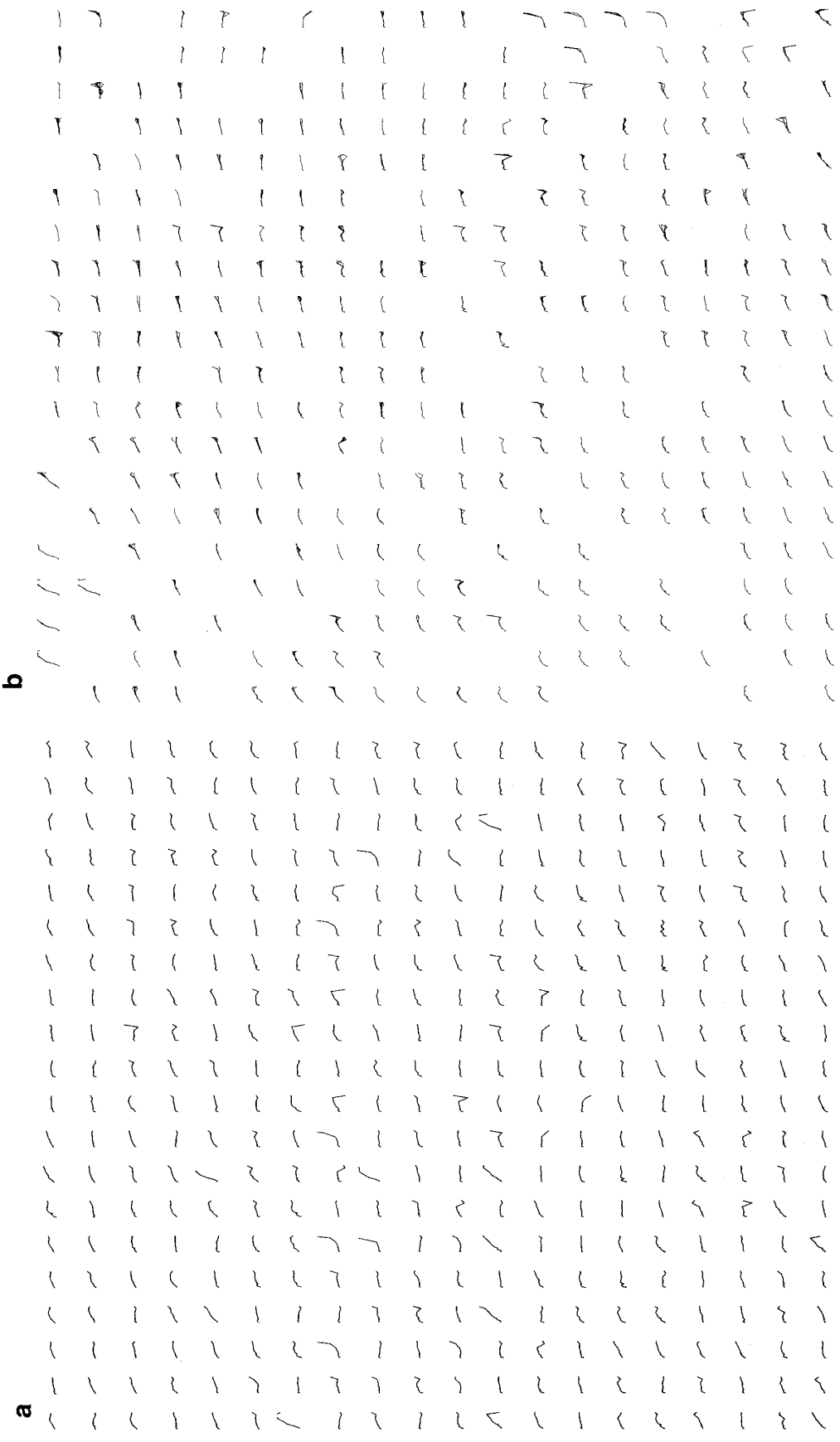

FIG. 5. The result of self-organization on a set of 13-color spectra, produced by a Self-Organizing type of Artificial Neural Network. (a) 400 randomly selected spectra from the 1386 that were input to the Self-Organizing Neural Network. (b) The 1386 spectra organized into groups of similar shapes. Notice that there may be multiple spectra in any grid location.

FIG. 6. The Self-Organizing Map (SOM) of the 1386 asteroid spectra of this study. (a) The SOM for the 13-point data (0.33–3.35 μm); (b) The SOM for the 11-point data (shortward of 3 μm). This is essentially the same kind of map as in Fig. 5b, except here every spectrum is represented by a small square instead of drawing the spectrum itself. One grid point in Fig. 5b corresponds to a 4 × 4 patch of small squares here. The white fences outline the cluster boundaries as detected by the Self-Oragnizing Map. The thickness of each fence is proportional to the degree of dissimilarity between the clusters that it separates. In order to compare our clusters with the Tholen taxonomical classes, we indicated the Tholen class designation of each spectrum by a color as shown on the wedge. The SOM clusters exhibit a remarkable agreement with the existing taxonomy, with a few minor exceptions that are described in the text. The squares that represent spectra of known wet objects are cross-hatched. The hydrated objects show a definite grouping across the various taxonomical types. Two distinct ''water groups'' are seen, one large group over M, C, B, and G types and one smaller group across the T and D types. The SOMs of the 13- and 11-color data are strikingly similar in structure. Details are discussed in the text.

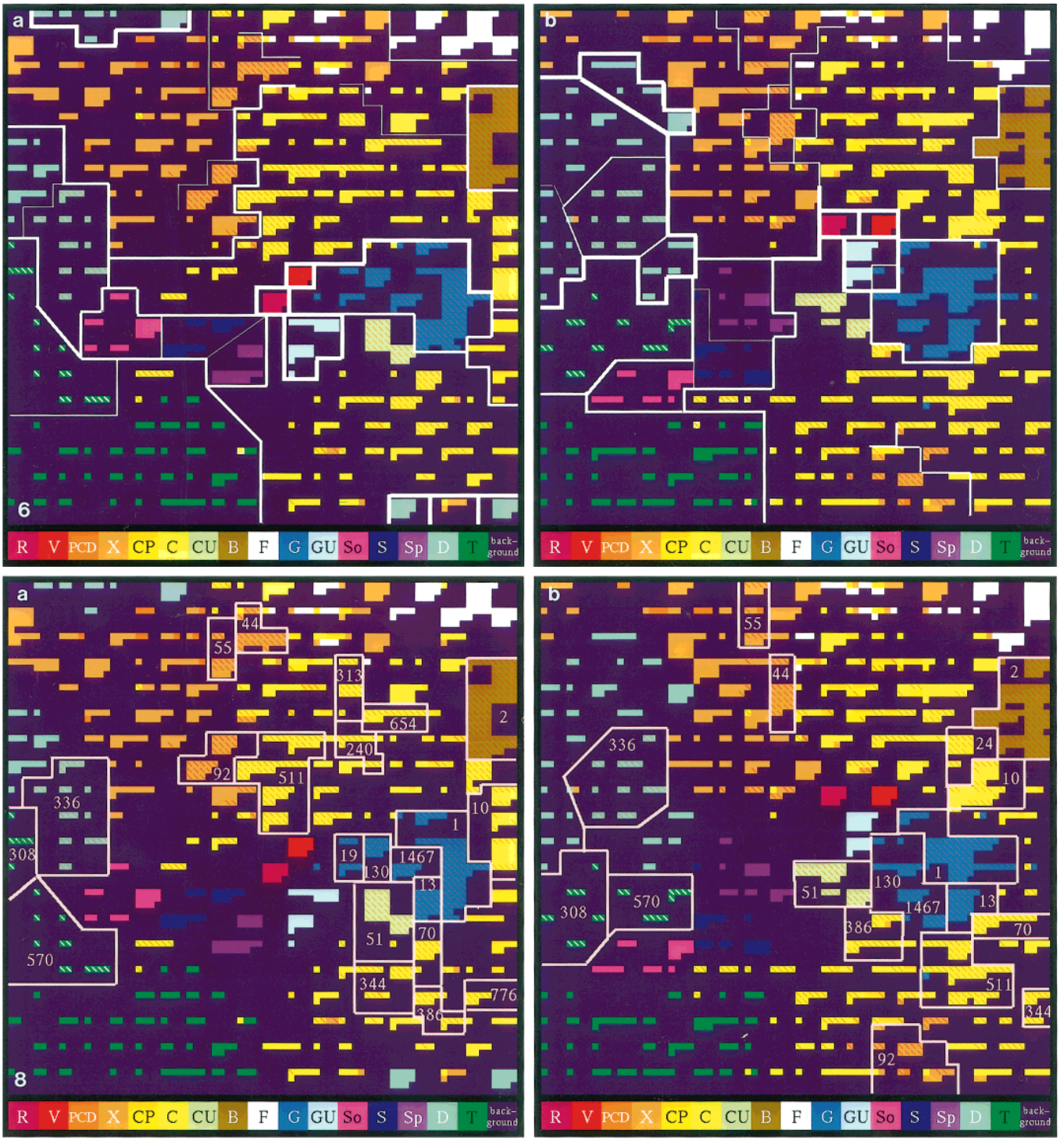

FIG. 8. The same as Fig. 6, without the cluster boundaries, and with several individual objects outlined. Each enclosed region contains spectra of the object indicated by its number. (a) Layout of objects in the 13-color SOM. (b) Layout of objects in the 11-color SOM. While the relative location of individual objects can differ considerably between the two maps, the ''water groups'' remain coherent.

For a comparison with the established taxonomy (Tholen 1984, Howell *et al.* 1994) each square was color-coded *after* the creation of this SOM, according to the taxonomical class designation of the object as given in the wedge in Fig. 6. The fences represent knowledge established by and then gleaned from the ANN while the color codes indicate the current accepted taxonomical type labels. The groups of colors exhibit a remarkable correspondence with the groups of squares within the cluster boundaries (white fences) established by the self-organizing ANN. This indicates that the ANN detected the same basic structure in the data as the generally accepted taxonomy. In case of multiple class labels (PCD, CP, CU, GU) the first letter gives the most probable class and the following letter(s) stand(s) for the next probable designation(s), after Tholen's (1984) convention. The X-class asteroids stand for M, E, and P types combined since these do not separate well in the absence of albedo. For this work, these asteroids are all treated as a single class, with albedo information not included. The upper middle of the SOM exhibits the least clear correspondence with the existing type designations.

The most conspicuous diversion in Fig. 6a is the group of Ds in the upper left and lower right edges. Both groups are delineated with thick fences indicating a very strong dissimilarity with the surrounding objects. The spectra in the upper left D group are all those of 944 Hidalgo and 1867 Deiphobus on the rightmost within the white borders. These spectra are different from the rest of the Ds, which are seen in the middle left main D cluster. 944 Hidalgo has the reddest slope of all spectra in this analysis. The difference to a typical D is illustrated in Fig. 7, which shows that the ANN detected a significant spectral shape difference. 1876 Deiphobus, although not quite as red as 944 Hidalgo, still has a significantly steeper spectrum than most D-type objects. The two D clusters in the lower right are split from the major D clusters by a wrap-around effect that is related to the finite size of the SOM. They contain all occurrences of 1172 Aneas (rightmost) and those of 721 Tabora. These are much less steep than 944 Hidalgo or 1867 Deiphobus but considerably redder than most other Ds. This variation among the D asteroids is not surprising when we take into account that none of these objects is a main belt D asteroid. 721 Tabora is a Cybele, with semimajor axis of 3.4 AU. 1867 Deiphobus and 1172 Aneas are Trojan asteroids, at a heliocentric distance of 5.2 AU. 944 Hidalgo is in an unusual asteroid in an eccentric orbit that crosses both Jupiter and Saturn. Howell (1995) finds a trend of redder slopes with increasing heliocentric distance among D asteroids, consistent with these results.

The olivine rich (So) and pyroxene rich (Sp) subdivisions of the S class, recently introduced into the taxonomy by Howell *et al.* (1994) as a refinement of the S class, also have a clear separation in these data, both 13- and 11-color (Fig. 6).

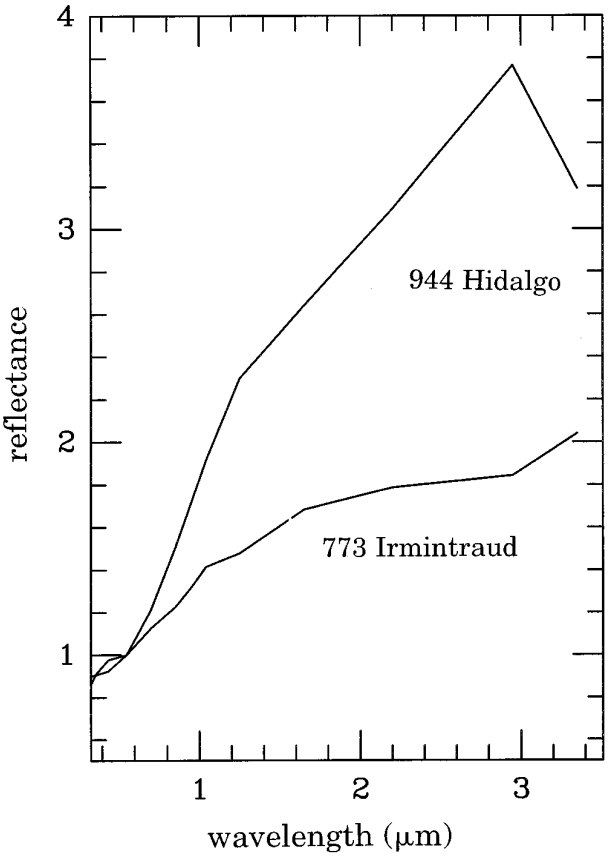

FIG. 7. Representative 13-color spectra from the groups of Ds that the ANN found strongly dissimilar. The upper curve is that of 944 Hidalgo, mapped in the upper left in Fig. 6a, separately from the rest of the Ds in the middle left of the SOM. The lower curve is that of 773 Irmintraud, one of the main-belt Ds.

The squares that represent spectra of known hydrated objects are cross-hatched in Fig. 6, and they form two coherent "water groups." One is on the middle left comprising Ds and Ts and the other is extending over most of the right half of the map. Both water groups stretch across taxonomical types. Notice how the hydrated and non-hydrated variants of the same types are separated by thin fences. For example, the wet Xs were mapped closer to the wet Cs than the dry Xs, and a thin line appears between them. The water clusters thus seem to be forming on top of the known taxonomy, adding a new dimension to the classification rather than scrambling the existing clusters.

The topology, i.e., the relative arrangement, of the 13-color spectra in Fig. 6a and the 11-color spectra in Fig. 6b is strikingly similar. Not only are the types clustered similarly but the hydrated spectra also show the same groupings. The group of 944 Hidalgo and 1867 Deiphobus spectra here are mapped adjacent to the other Ds on the upper right of the main D cluster. The spectra of 1172 Aneas and 721 Tabora do not suffer from the wraparound

effect as in Fig. 6a and they are also mapped adjacent to the lower right and lower left of the main D cluster, respectively. However, these groups are just as strongly separated from the rest of the Ds as in the 13-color case. It is interesting to compare the mapping of individual objects between the 13-color and the 11-color SOM. In Figs. 8a and 8b groups of squares that belong to the same one object are outlined in pink, marked with the asteroid number. These outlines are independent of the fences in Fig. 6. While the white lines there represent knowledge gleaned from the ANN, the pink lines here merely overlay information known to us, namely that the encircled squares all represent spectra of the same asteroid identified by its number. Between the 13- and 11-color SOM some objects map differently. For example, 92 Undina and 511 Davida moved to the lower right from the middle. Still, the water group remained coherent.

We can conclude from the unsupervised classification that our data seem to exhibit a very similar structure with respect to hydration feature(s) in the 13-color and the 11-color data. In other words, even without the 3 μm water band the ANN detects some feature(s) that hold the spectra of the known hydrated objects together. This gives us confidence that some consistent relationship may exist between the 3 μm band and certain spectral properties shortward of 3 μm.

5. PREDICTION OF WATER FROM THE VIS–NIR WITH SUPERVISED CLASSIFICATION

After we established reliable water clusters, the next step, the real test of consistency, was to train the hybrid ANN described in Section 3.1.2 for the water designation of objects that we had firm knowledge of in supervised mode. The output layer had two nodes, one to indicate wet objects and one for the dry objects. First we tested the ANN's capability to learn from a set of example spectra and to use the derived knowledge to make predictions for unseen ones, using the 13-color data. Of the original spectra, 85% were selected for training; the remaining 15% were set aside as ''unknown'' test spectra. Because of the small number of samples the representation of taxonomic types and especially that of ''wet'' and ''dry'' across all types is rather poor and uneven. Therefore a jackknifing approach was helpful, which means that the training and test was performed seven times, with different 85/15% picked for training and test sets each time. This ensured that in seven rounds every spectrum participated once as an unseen pattern. After the exclusion of obviously inconsistent or very doubtful information, 97 spectra remained for this exercise; 83 were selected for training and 14 were used as test patterns, in each jackknife run. Inconsistent information here means that some of the spectral shapes in the 13-color data do not show a definite water band even though the objects that these spectra represent are believed to contain water. Because asteroids here are considered either hydrated or anhydrous, objects with shallow absorption features and/or relatively low signal-to-noise and/or spectral variation may result in data that sometimes appears hydrated and sometimes anhydrous. We excluded such spectra from the supervised classification to avoid the possible confusion that these may cause. Results are shown in Table II. The ANN perfectly learned the water labels of the training spectra and was able to generalize from that knowledge well. These results were obtained after 15K supervised training steps and changed little if at all for a larger number of training steps. The prediction rates are seemingly poor in the second column. However, the situation is much better. The ANN has the capability to say that it was unable to make a decision for class designation. The rate of such undecided cases are listed in the fourth column. If we calculate how often the ANN gave the correct prediction when it did make a decision, we get the high rates shown in the last column.

Then we repeated the supervised classification for the 11-color data. Everything was the same as in the previous step except all spectra were used in their truncated, 11-point form. The hybrid ANN this time was built on the 11-color SOM in Fig. 6b. The results are shown in Table III. Again, the learning rate is perfect. The last column is the proof that the ANN detected a definite correlation of some features in the VIS–NIR to the 3 μm band since it could make very consistent predictions from the 11-color data.

What the high percentage of the undecided cases tells us is that we really only have a small amount of data, too little for the ANN to derive firm and completely generalized knowledge of what ''hydrated'' means, across so many taxonomical types and spectral shape variations. The consistent predictions for those cases when a definite decision was possible make the knowledge derived by the ANN a valuable tool that can be put to use as it is, since in those cases we can have high confidence in the ANN's prediction. We will be able to improve the number of cases for which prediction is possible, and with that the overall prediction rate, continuously as we collect more and more data.

It is worth noting that the same spectra that remained unclassified in the 11-color scheme were also unclassified in the 13-color scheme (except for two that were undecided only in the 11-color runs). In addition, the 13-color classification resulted altogether in 11 more undecided spectra than the 11-color case. This may be explained by the fact that the spectral shape variation across taxonomical types is much larger when the 3-μm water band is included and therefore a learning device may require more examples to recognize ''wet'' and ''dry.''

TABLE II
The Results of the Supervised Classification on the 13-Color Data

jackknife number	rate of correct predictions	rate of wrong predictions	rate of undecided cases	correct of predicted cases
		Test on training spectra		
1–4, 7	100.0 %	0.0 %	0.0 %	100.0 %
5–6	99.0 %	1.0 %	0.0 %	99.0 %
average	99.7 %	0.3 %	0.0 %	99.7 %
		Test on unseen spectra		
1	35.7 %	7.1 %	57.1 %	83.3 %
2	30.8 %	0.0 %	69.2 %	100.0 %
3	30.8 %	0.0 %	69.2 %	100.0 %
4	46.2 %	0.0 %	53.8 %	100.0 %
5	30.8 %	0.0 %	69.2 %	100.0 %
6	23.0 %	0.0 %	76.9 %	100.0 %
7	35.7 %	0.0 %	61.5 %	100.0 %
average	33.3 %	1.0 %	65.3 %	97.6 %

Note. Of the original 126 observed spectra, 97 were used with the exclusion of obvious inconsistent information. 83 spectra served as training samples and 14 spectra were used as "unseen" test spectra, in each of seven jackknife cases. The seven selections of unseen spectra cover the entire set. Results of the individual jackknife runs and their averages are shown. The seemingly low rate in the second column is explained by the large number of cases in which no decision could be made because of insufficient training information. The last column indicates that in those cases when decision could be made the success is high.

TABLE III
The Results of the Supervised Classification on the 11-Color Data

jackknife number	rate of correct predictions	rate of wrong predictions	rate of undecided cases	correct of predicted cases
		Test on training spectra		
1–7	100 %	0 %	0 %	100 %
		Test on unseen spectra		
1	50.0 %	7.1 %	42.9 %	87.5 %
2	38.5 %	15.4 %	46.2 %	71.4 %
3	46.2 %	7.7 %	46.2 %	85.7 %
4	76.9 %	0.0 %	23.1 %	100.0 %
5	38.5 %	0.0 %	61.5 %	100.0 %
6	53.8 %	0.0 %	46.2 %	100.0 %
7	42.9 %	7.1 %	50.0 %	85.7 %
average	49.5 %	6.3 %	45.2 %	90.0 %

Note. The same spectra were used for training and test as in Table II, except truncated to 11 points.

TABLE IV
Summary of All Classification Results

classification run	correct predictions	incorrect predictions	undecided cases	correct of predicted cases
		Test on unseen spectra		
13-color	33.3 %	1.0 %	65.3 %	97.6 %
11-color	49.5 %	6.3 %	45.2 %	90.0 %
8-color	51.0 %	9.6 %	39.4 %	82.9 %
10-color	62.0 %	38.0 %	0.0 %	62.0 %
Vilas scheme	57.4 %	42.5 %	0.0 %	57.4 %

Note. These numbers are averages of the same seven jackknife runs as in Tables II and III, for every channel selection shown in Fig. 3.

6. WHAT ARE THE CORRELATING FEATURES?

Vilas (1994) argued that the presence of a 0.7-μm absorption band was an indicator of hydrous state, as in her investigation this feature occurred in 80% of the spectra that also had a 3-μm band. She used the empirically established condition that if

$$(R_{0.701} - ((R_{0.853} - R_{0.550})\ 0.4984))/R_{0.550} < 0.990,$$

then the 0.7-μm absorption was present.

Vilas focused on one particular feature, the relative band depth at 0.7 μm. Her training population included 31 spectra of C, D, F, G, and P type asteroids (no M, E, S, T) from which the 80% correlation between the 3-μm band and the 0.7-μm feature was derived. This data set contained roughly 50–50% of hydrated and anhydrous spectra. We use the entire spectrum shape with no assumption as to what part of it carries correlating information with the 3-μm water band. Our training population includes samples of all classes therefore it is less biased for wet- and dry-type asteroids than Vilas' data. Our training set is also well balanced for the overall number of wet and dry samples (48 and 46 occurrences, respectively).

The iron feature near 0.7 μm might provide a clue to the presence of hydrated minerals for the C-type asteroids, but this feature is not present in the E-, M-, and P-type asteroids. Vilas (1994) also points out that her formula fails for M-class hydrated asteroids. The ANN prediction rates for the E, M, and P classes are perfect when prediction is made while 73% of the predicted cases are correct for C spectra. However, we have only slightly more than half as many E, M, and P asteroid spectra as Cs in our study, and the ratio of undecided cases is significantly higher for E, M, and P types, which makes this comparison somewhat inconclusive.

To test the importance of the 0.7-μm feature and of other parts of the spectrum, we ran the same jackknives as before but with various parts of the spectrum eliminated. The spectral selections are shown in Fig. 3. The results, averaged from the seven jackknife runs for each case, are listed in Table IV. First, the 0.7 point was eliminated from the spectra (10-color data in Fig. 3). Row 4 in Table IV indicates that there was not one undecided case and that the prediction rate was still significantly higher than 50% (62%) so that it is unlikely a mere random hit/miss. We also tested our spectra with Vilas' formula, with a 57.4% success shown in row 5 in Table IV. The much lower than 80% success here reflects the fact that our data contain spectral types (E, M, P, S) in which no 0.7-μm band is present while both wet and dry objects occur among them. Finally, we ran the jackknives on the 8-color data (row 3 of Table IV) to see how much of the prediction capability is lost with the elimination of the J, H, and K bands.

The prediction rate fell strongly by the elimination of the 0.7-μm point which suggests that this feature plays a significant role in the correlation. It also increased the certainty of the network in decision making. This is analogous to a less educated person being more certain in decision making based on simplified facts, but also making more incorrect decisions due to lack of relevant information.

The trend from the 13- to 11- to 8- to 10-color cases and to Vilas' is also illustrated in Fig. 9. Prediction rate falls, and uncertainty simultaneously decreases. Elimination of the J, H, and K bands causes a 7% drop in the prediction rate. The difference between the 8-color and the Vilas scheme results, however, suggests that significant contribution comes from the ECAS range, from elsewhere

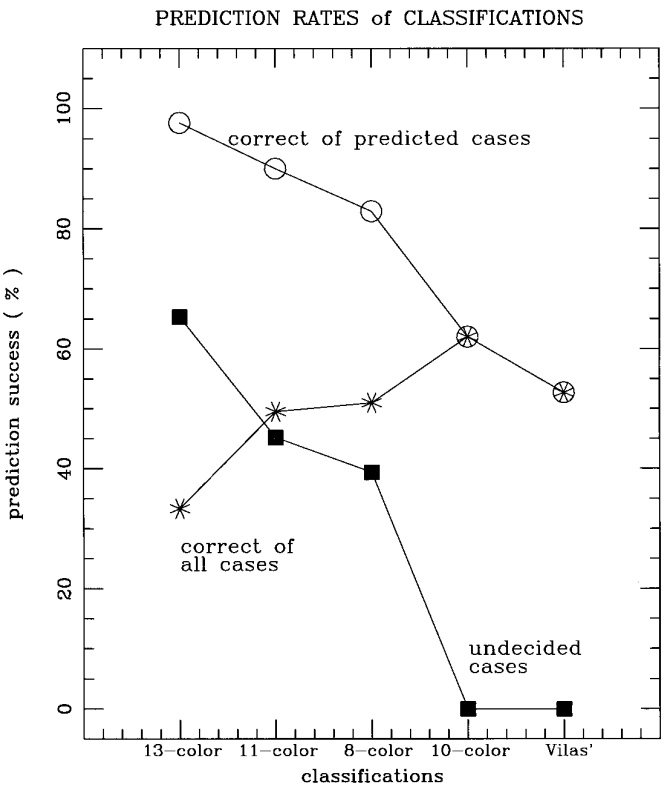

FIG. 9. The prediction tendencies across the 13-, 11-, 8-, and 10-color and Vilas' data. The data sets are defined in Fig. 3. The high correct ANN rate of the predicted cases slowly drops through the 13-, 11-, and 8-color data sets and has a significant drop for the 10-color data, while the number of undecided cases is decreasing and drops to none for the 10-color set. Access to more parameters (i.e., 13-color data) requires more complex decision making, but the available samples may not be quite enough to derive the effects of many parameters. Hence, the ANN remains undecisive for the largest number of spectra. Fewer parameters (11-color case) result in clearer "rules" that the ANN can derive, and in fewer undecided cases. However, the rate of correct decisions also decreases as the ANN is ignorant of some relevant information. This tendency continues through the 8-color set. The huge drop for the 10-color data indicates that the 0.7 μm point is a relevant indicator of the hydration state and that it contains information that is complementary to the other sets. Therefore, its absence makes decisions simpler and predictions poorer. The Vilas scheme was run on our data for comparison.

than the 0.7-μm point. The correctly predicted cases are very consistently preserved through the 8-, 11-, and 13-color tests. In the 10-color tests, wrong decisions are almost exclusively given for those spectra that are undecided in the 11-color case. There are, however, large opposite biases in the prediction failures of the 10-color and Vilas scheme tests as shown in Table V. The 10-color test has a strong tendency to err on the wet side while Vilas' formula errs on the dry side in a similar number of cases. This indicates that the 0.7-μm band and other parts of the ECAS range contain complementary

TABLE V
Prediction Biases in the Wrong Predictions for the Various Data Sets

classification	# cases	# of decided	Wet for Dry	Dry for Wet
11-color ANN	94 (76)	51 (40)	3 (3)	2 (2)
8-color ANN	94 (76)	58 (50)	2 (2)	6 (6)
10-color ANN	94 (76)	94 (76)	33 (23)	5 (5)
Vilas'	94 (76)	94 (76)	5 (5)	35 (30)

Note. In the case of the 8- and 11-color data, errors are roughly the same in each direction. For the 10-color data (i.e., 11-color data without the 0.7 μm point), most failures are predictions of "Wet" when the object is "Dry." Vilas' formula errs on the opposite side, to the same large extent. This, together with the classification success of the 8-color data set in Table IV suggests that the 0.7 μm feature and other parts of the ECAS range carry complementary information of the hydration state. Numbers in parentheses show rates without E, M, and S types.

information about the hydration state. Feierberg *et al.* (1985) showed a correlation between the U-B color and hydration state for C and G asteroids, which may also be recognized by the ANN. However, this feature is not present in E, M, and P asteroid spectra.

Additional, more detailed analysis could be done to pinpoint the contributions of individual channels by further sectioning the spectral range and experimentally determining the relative contributions from various parts of the spectrum. "Dissecting" the artificial brain would be another possible, direct method. Examination of the internal state of the trained ANN can reveal its knowledge if a sufficiently powerful and sophisticated approach is used. For a full and clear identification with either method, however, more data may be needed than the presently available amount.

7. SUMMARY AND FUTURE WORK

We have analyzed spectra from 126 observations of 80 asteroids. We conducted our investigations on the same data with and without the 3-μm water band in order to research correlations between the 3-μm signature and other VIS–NIR features. The internal structure of these data shows a general good agreement with Tholen's taxonomy. An additional grouping according to the presence of water was found in both versions of the data. The water groups and the known taxonomical groups are very similar in the two data sets, which supports the existence of VIS–NIR indicators for the presence of water: that water may be predicted from the shorter wavelength (<3 μm) part of the spectra. We have constructed an Artificial Neural Net tool that predicts the hydration state from the <3 μm part of the spectrum with 90% accuracy.

The 0.7-μm point is an important component of the correlating information. However, there seems to be significant contribution within the ECAS range outside of the 0.7-μm point and possibly some lesser contribution from the J, H, and K range, too. A trend can be seen that elimination of the 0.7-μm point causes erring on the wet side in the predictions while using only the 0.7-μm relative band-depth leads to erring on the dry side. Clearly, there is complementary information in these two cases, the combination of which more accurately characterizes the hydration state than one or the other alone.

Due to the small number of the 3-μm observations, there are biases in the data. This also makes our training sets less than ideally represent wet and dry across so many taxonomical types, which results in many undecided cases in the ANN runs. The number of objects to which we can apply this tool is presently limited by the available variety of data for training. This situation is expected to improve as additional data become available.

ACKNOWLEDGMENTS

We thank the J. F. Bells for their thoughtful reviews and helpful suggestions. This research was partially supported by the Planetary Image Research Laboratory (PIRL) and by the Lunar and Planetary Laboratory (LPL) of the University of Arizona. L. Lebofsky, E. Howell, and A. Rivkin were partially supported by NASA Grants NAGW 1146 and NAGW 1975. The computing facilities of LPL and PIRL and contributions to this work by NASA Space Grant Intern Michael Ammerlaan are gratefully acknowledged. The Khoros image processing environment (Rasure and Young 1992) was used to produce the image figures.

REFERENCES

Barucci, M. A., M. T. Capria, A. Coradini, and M. Fulchignoni 1987. Classification of asteroids using G-mode analysis. *Icarus* **72,** 304–324.

Bell, J. F., P. D. Owensby, B. R. Hawke, and M. J. Gaffey 1988. The 52-color asteroid survey: Final results and interpretation. *Lunar Planet. Sci.* **XIX,** 57.

Benediktsson, J. A., J. R. Sveinsson, and K. Arnason 1994. Classification of very-high-dimensional data with geological applications. In *Proc. MAC Europe 91, Lenggreis, Germany, 4–6 October, 1994,* pp. 13–18.

Benediktsson, J. A., P. H. Swain, O. K. Ersoy, and D. Hong 1990. Classification of very high dimensional data using neural networks. In *IGARSS'90 10th Annual International Geoscience and Remote Sensing Symposium II,* pp. 1269–1272.

Britt, D. T., L. A. Lebofsky, and E. S. Howell 1992. 3-μm observations of C-class asteroids. *Bull. Amer. Astron. Soc.* **24,** 940. [Abstract]

Britt, D. T., A. S. Rivkin, E. S. Howell, and L. A. Lebofsky 1994. Observations of "dry" C-class asteroids. *Bull. Amer. Astron. Soc.* **26,** 1175. [Abstract]

Burbine, T. H. 1991. *Principal Component Analysis of Asteroid and Meteorite Spectra from 0.3 to 2.5 μm.* Master's dissertation, University of Pittsburgh.

Burbine, T. H., and J. F. Bell 1993. Asteroid taxonomy: Problems and proposed solutions. *ACM* **111,** 49.

Chapman, C. R. 1987. The asteroid belt: Compositional structure and size distributions. *Bull. Amer. Astron. Soc.* **19,** 839. [Abstract]

Feierberg, M. A., L. A. Lebofsky, and H. P. Larson 1981. Spectroscopic evidence for aqueous alteration products on the surfaces of low-albedo asteroids. *Geochem. Cosmochem. Acta* **45,** 971–981.

Feierberg, M. A., L. A. Lebofsky, and D. J. Tholen 1985. The nature of C-class asteroids from 3-μm spectrophotometry. *Icarus* **63,** 183–191.

Gaffey, M. J., J. F. Bell, R. H. Brown, T. Burbine, J. L. Piatek, K. L. Reed, and D. A. Chakey 1993. Mineralogical variations within the S-type asteroid class. *Icarus* **106,** 573–602.

Hayken, S. 1995. *Neural Networks. A Comprehensive Foundation.* Macmillan, New York.

Hepner, G. F., T. Logan, N. Ritter, and N. Bryant 1990. Artificial neural network classification using a minimal training set: Comparison to conventional supervised classification. *Photogrammetric Eng. Remote Sensing* **56**(4), 469–473.

Howell, E. S. 1995. *Probing Asteroid Composition Using Visible and Near-Infrared Spectroscopy.* Ph.D. dissertation, University of Arizona.

Howell, E. S., L. A. Lebofsky, M. C. Nolan, and E. M. Alvarez del Castillo 1992. Compositional trends among outer belt asteroids. *Bull. Amer. Astron. Soc.* **24,** 940–941.

Howell, E. S., E. Merényi, and L. A. Lebofsky 1994. Classification of asteroid spectra using a neural network. *J. Geophys. Res. Planets* **99** (E5), 10,847–10,865.

Huang, W., and R. Lippman 1987. Comparisons between neural net and conventional classifiers. In *IEEE First International Conference on Neural Networks IV, San Diego,* pp. 485–494.

Jones, T. D., L. A. Lebofsky, J. S. Lewis, and M. S. Marley 1990. The composition and origin of the C, P, and D asteroids: Water as a tracer of thermal evolution in the outer belt. *Icarus* **88,** 172–192.

Kohonen, T. 1988. *Self-Organization and Associative Memory.* Springer–Verlag, New York.

Lebofsky, L. A. 1980. Infrared reflectance spectra of asteroids: A search for water of hydration. *Astron. J.* **85,** 573–585.

Lebofsky, L. A., T. D. Jones, P. D. Owensby, M. A. Feierberg, and G. J. Consolmagno 1990. The nature of low albedo asteroids from 3-μm spectrophotometry. *Icarus* **83,** 12–26.

Merényi, E., R. B. Singer, and W. H. Farrand 1993. Classification of the LCVF AVIRIS test site with a Kohonen artificial neural network. In *Proc. Fourth Airborne Geoscience Workshop, Washington, D.C., Oct. 25–29.* JPL Publication 93-26 1993, Vol. 1, pp. 117–120.

Merényi, E., R. B. Singer, and J. S. Miller 1996. Mapping of spectral variations on the surface of Mars from high spectral resolution telescopic images. *Icarus* **124,** 280–295.

NeuralWare, Inc. 1991. *Neural Computing,* p. 317. NeuralWorks Professional II Manuals, NC.

Ninomiya, Y., and I. Sato 1990. Estimation of SiO_2 content using thermal infrared reflectance spectra of rocks. In *Proceedings 10th Annual International Geoscience and Remote Sensing Symposium II,* pp. 979–982.

Pao, Y. H. 1989. *Adaptive Pattern Recognition and Neural Networks.* Addison-Wesley, Reading, MA.

Paola, J. D., and R. A. Schowengerdt 1994. Comparison of neural network to standard techniques for image classification and correlation. In *Proceedings International Geoscience and Remote Sensing Symposium, Caltech, Pasadena, CA, August 8–12, 1994, III,* pp. 1404–1405.

Rasure, J. R., and M. Young 1992. An open environment for image processing software development. In *Proceedings of the SPIE/IS& T Symposium in Electronic Imaging, February 14, 1992,* Vol. 1659 pp. 300–310.

Rivkin, A. S., E. S. Howell, D. T. Britt, L. A. Lebofsky, M. C. Nolan, and D. D. Branston 1995. 3-μm spectrophotometric survey of M and E-class asteroids. *Icarus* **117,** 90–100.

Tedesco, E. F. 1989. Asteroid magnitudes, UBV colors, and IRAS albedos and diameters. In *Asteroids II* (R. P. Binzel, T. Gehrels, M. S. Matthews, Eds.), pp. 1090–1138. Univ. of Arizona Press, Tucson.

Tholen, D. J. 1984. *Asteroid taxonomy from cluster analysis of photometry.* Ph.D. dissertation, University of Arizona, Tucson.

Tholen, D. J. 1989. Asteroid taxonomic classification. In *Asteroids II* (R. P. Binzel, T. Gehrels, M. S. Matthews, Eds.), pp. 1139–1150. Univ. of Arizona Press, Tucson.

Vilas, F. 1994. A cheaper, faster, better way to detect water of hydration on Solar System bodies. *Icarus* **111,** 456–467.

Wang, Y., and D. L. Civco 1995. Artificial neural networks in high dimensional spatial data classification: A performance evaluation. In *ACMS/ASPRS Annual Convention & Exposition Technical Papers, Charlotte North Carolina, February 27–March 2, 1995,* Vol. 3, pp. 662–671.

Zellner, B., D. J. Tholen, and E. F. Tedesco 1985. The eight-color asteroid survey: Results for 589 minor planets. *Icarus* **61,** 355–416.